

## Spin Excitations in a $4f - 3d$ Heterodimer on MgO

A. Singha,<sup>1,2,3</sup> F. Donati,<sup>1,2,3</sup> F. D. Natterer,<sup>2,4</sup> C. Wäckerlin,<sup>2,5</sup> S. Stavrić,<sup>6</sup> Z. S. Popović,<sup>6</sup>  
 Ž. Šljivančanin,<sup>6,7</sup> F. Patthey,<sup>2</sup> and H. Brune<sup>2</sup>

<sup>1</sup>Center for Quantum Nanoscience, Institute for Basic Science (IBS), Seoul 03760, Republic of Korea

<sup>2</sup>Institute of Physics, École Polytechnique Fédérale de Lausanne, Station 3, CH-1015 Lausanne, Switzerland


<sup>3</sup>Department of Physics, Ewha Womans University, Seoul 03760, Republic of Korea

<sup>4</sup>Physik-Institut, Universität Zürich, Winterthurerstrasse 190, CH-8057 Zürich, Switzerland

<sup>5</sup>Nanoscale Materials Science, Empa, Swiss Federal Laboratories for Materials Science and Technology, 8600 Dübendorf, Switzerland

<sup>6</sup>Vinča Institute of Nuclear Sciences, University of Belgrade, P.O. Box 522, RS-11001 Belgrade, Serbia

<sup>7</sup>Texas A&M University at Qatar, P.O. Box 23874, Education City, Doha, Qatar

 (Received 8 July 2018; revised manuscript received 18 October 2018; published 18 December 2018)

We report on the magnetic properties of HoCo dimers as a model system for the smallest intermetallic compound of a lanthanide and a transition metal atom. The dimers are adsorbed on ultrathin MgO(100) films grown on Ag(100). New for  $4f$  elements, we detect inelastic excitations with scanning tunneling spectroscopy and prove their magnetic origin by applying an external magnetic field. In combination with density functional theory and spin Hamiltonian analysis, we determine the magnetic level distribution, as well as sign and magnitude of the exchange interaction between the two atoms. In contrast to typical  $4f - 3d$  bulk compounds, we find ferromagnetic coupling in the dimer.

DOI: [10.1103/PhysRevLett.121.257202](https://doi.org/10.1103/PhysRevLett.121.257202)

Many alloys combining transition metal (TM) elements of the first row with rare earth (RE) elements are widely used as permanent magnets due to their large magnetic anisotropy and remanent magnetization. The coupling between the spins of these elements can give rise to complex magnetic structures that exhibit rich phase diagrams [1]. This is due to the indirect exchange interaction between the  $4f$  orbitals of the RE and the  $3d$  orbitals of the TM mediated by the *spd* conduction electrons [2]. In addition, the magnetic order of RE-TM alloys is strongly affected by structural relaxations and surface effects [3]. Both become particularly important when the size of the magnet reaches atomic dimensions [4–8].

Understanding the magnetic level distribution and, therefore, the origin of magnetic anisotropy is important for the rational design of prototypical nanomagnets. The splitting of the low energy levels can be investigated using scanning tunneling microscopy (STM) and spin-excitation spectroscopy (SES) [9]. However, the detection of spin-excitations in  $4f$  atoms and  $4f$  single molecule magnets is very challenging due to the vanishing contribution of the  $4f$  electrons to the tunnel current as a result of their strong localization [10,11], and reading the magnetic state of adsorbed RE atoms and islands is possibly enabled by the exchange interaction with the  $5d$  shell [10,12]. Accordingly, spin-excitations have not been reported in  $4f$  containing nanostructures, including single molecule magnets, apart from claims that, however, were not substantiated by demonstrating their Zeeman shifts [13–15].

Also, for some of the claimed systems [14], the inelastic features and associated magnetic properties could not be reproduced [11,16]. In contrast to the strongly localized  $4f$  electrons, the  $3d$  orbitals of TM atoms are more directly probed by tunneling electrons, and therefore, they often exhibit large SES cross sections [17]. In order to access the magnetism of  $4f$  elements via SES, we combine one RE atom with one TM atom and study the magnetism of this heterodimer, which is also a model system for probing the  $4f - 3d$  exchange coupling at the atomic scale.

We report on the magnetic properties of HoCo heterodimers on MgO(100) thin films grown on Ag(100) [18]. The properties of Ho and Co on MgO are particularly intriguing: Ho on MgO is the first discovered single atom magnet which exhibits a magnetic moment that is close to its highest possible value [33–35], whereas Co on the same surface exhibits the largest magnetic anisotropy energy [17]. The MgO(100) thin films grown on metal surfaces are ideal substrates as MgO decouples the magnetic states of adsorbates from the scattering of substrate electrons and soft phonons [33,36]. For HoCo dimers, we observe two pairs of spin-excitations at  $\pm 8$  and  $\pm 20$  meV, for which we develop an effective spin Hamiltonian (SH) [18] using minimal input from our density functional theory (DFT) calculations [18]. The SH model reproduces the magnetic field dependent conductance steps. In agreement with DFT, this model finds collinear ferromagnetic coupling between Ho and Co. The DFT inferred adsorption site is also in agreement with experiment. Using SH, we determine the

magnetic level spectrum of HoCo and the relative contribution of the two elements to the experimentally detected spin excitations.

The Ho and Co atoms were codeposited onto the cold substrates, in the measurement position of our 0.4 K,  $\pm 8$  T home-built STM [37]. This yields predominantly individual Ho and Co atoms, but also the occasional formation of homodimers and heterodimers. In order to unequivocally distinguish the different species, we prepared samples separately with only Ho or only Co. Each species has characteristic inelastic conductance ( $dI/dV$ ) steps and/or apparent heights. The homodimers, Ho<sub>2</sub> and Co<sub>2</sub>, show intense  $dI/dV$  steps located at  $\pm 85$  and  $\pm 13$  meV, respectively (Figs. S1 and S2 [18]). Figure 1(a) shows an STM image of the remaining four species. Isolated Ho atoms adsorb on top of O (Ho<sup>top</sup>) or bridge sites (Ho<sup>br</sup>) of the MgO(100) lattice [38]. They are discerned by their distinct apparent heights [Fig. 1(b)]; neither one has observable inelastic conductance steps [Fig. 1(e)]. Isolated Co atoms adsorb on top of O only [38] and are clearly identified by their  $dI/dV$  steps at  $\pm 58$  meV, reminiscent of their high magnetic anisotropy [17]. The apparent height of the HoCo dimer is distinct from Ho<sup>br</sup>, Ho<sup>top</sup>, and Co atoms [Fig. 1(b)], and it possesses an “egglike” footprint with its axis aligned along the MgO (100) lattice directions [Fig. 1(c)]. This shape, as well as the location of the dimer, are in agreement with the adsorption geometry inferred from DFT, where Ho and Co adsorb on two adjacent O sites with vertical distances of 2.26 and 1.89 Å [Fig. 1(d)].

The spectroscopic fingerprints of the heterodimer are conductance steps at  $\pm 20$  meV [Fig. 1(e)]. Their magnetic origin becomes evident from their linear shift in an out-of-plane external magnetic field [Fig. 2(a)]. This spin excitation is markedly different than the behavior of individual Ho and Co atoms on the same substrate, unlike the case of Fe-Ho pairs adsorbed on Pt(111), where the spin excitation of the Fe atom remains unchanged upon approaching the Ho atom to 4.24 Å distance [11]. Figure 2(b) displays the magnetic field and MgO thickness-dependent excitation energies for several HoCo dimers. From a linear fit to the step energy  $E(H) = g\mu_0 H \Delta m \mu_B$  [Fig. 2(b)], we extract the effective Landé  $g$  factor of  $3.1 \pm 0.3$  assuming  $\Delta m = \pm 1$  (Tables I and II of Supplemental Material [18]), where  $\Delta m$  is the change in the out-of-plane component of the total magnetic moment. The large mean value of  $g$  indicates the presence of a sizable orbital moment, consistent with a previous report for Fe atoms on MgO [39].

As can be seen from Fig. 2(b), the step energy depends strongly on MgO thickness (i.e., it moves to lower energy by 1.7 meV on thicker MgO layers) and, also, weakly on the local environment of a given dimer (variance of 0.2 meV for the dimer shown with gray triangles). According to DFT, the adsorption of the HoCo dimers leads to sizeable distortions of the underlying MgO lattice. These distortions

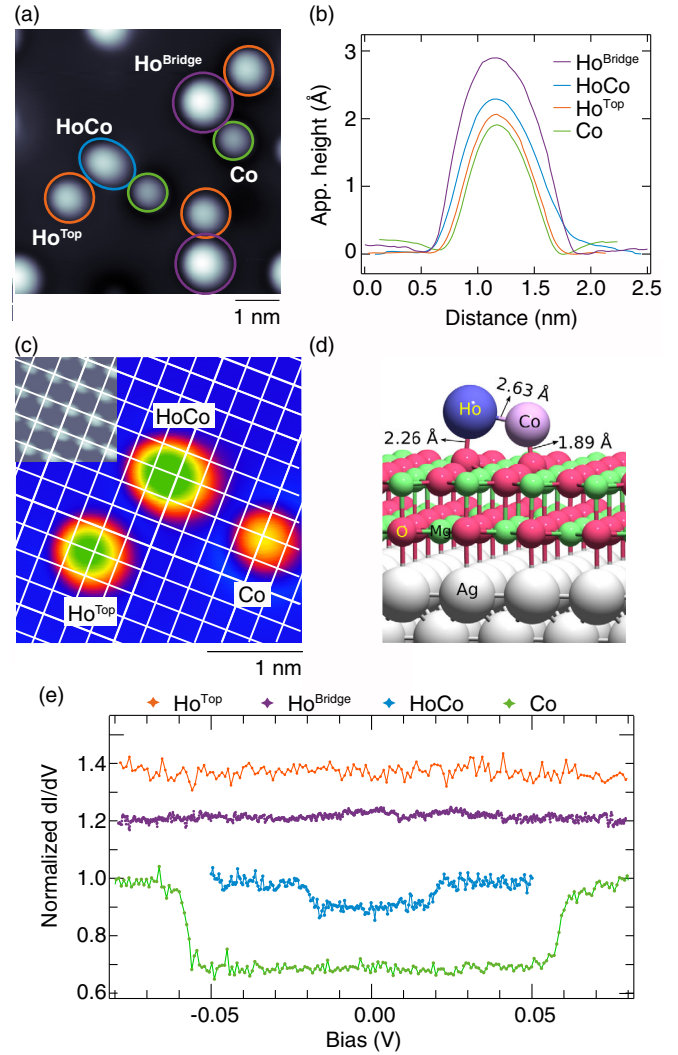


FIG. 1. Identification of HoCo dimers and detection of their spin excitations. (a) STM image and (b) apparent height profiles of HoCo dimer and individual Ho<sup>top</sup>, Ho<sup>br</sup>, and Co atoms. (c) STM image showing the characteristic elliptical shape of a HoCo dimer in comparison with the more symmetric shape of individual Ho and Co atoms [(a)–(c)]  $V_t = 100$  mV,  $I_t = 50$  pA, and  $\mu_0 H = 6$  T,  $T = 4.3$  K]. Inset: atomic resolution image of 2 ML MgO with O imaged bright ( $V_t = 10$  mV,  $I_t = 8$  nA). The white grid shows the O sublattice [38]. (d) DFT calculated adsorption geometry of HoCo. (e)  $dI/dV$  of HoCo dimer ( $V_t = 40$  mV,  $I_t = 250$  pA), Ho<sup>top</sup>, Ho<sup>br</sup>, and Co atoms ( $V_t = 100$  mV,  $I_t = 500$  pA). All spectra:  $V_{\text{mod,ptp}} = 1$  mV,  $\mu_0 H = 1$  T,  $T = 4.3$  K. For clarity, Ho<sup>top</sup> and Ho<sup>br</sup> spectra are vertically offset by 0.2 each.

as well as the crystal fields for 1 and 2 ML MgO/Ag(100) are different. This leads to the lower excitation energies observed for HoCo dimers adsorbed on thicker MgO films. Similar thickness dependent behavior was also observed for Fe atoms on MgO [40].

We expect two types of magnetic excitations in dimers, one where the total magnetic moment  $\hat{S}$  changes and one where its projection  $\hat{S}_z$  does [41]. The fact that only one

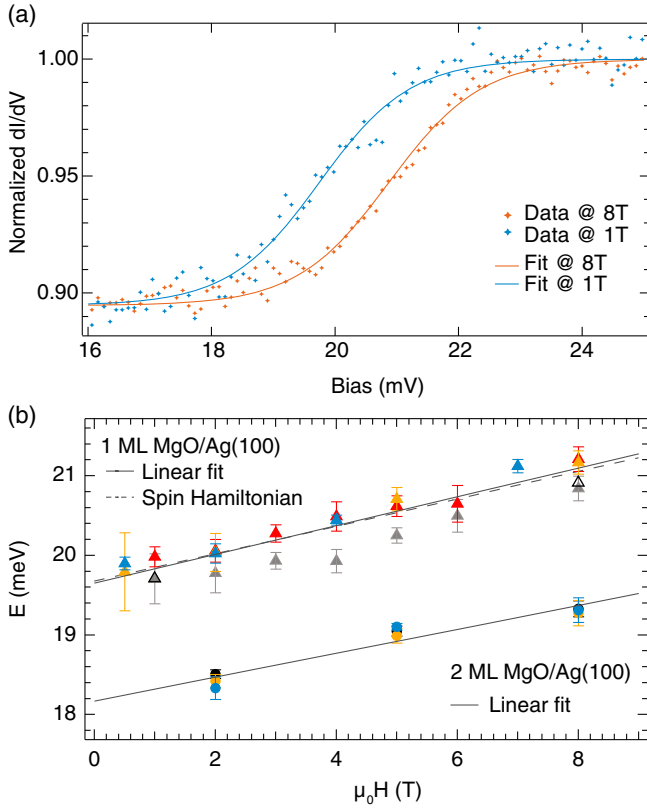


FIG. 2. (a) Magnetic field dependence of the  $dI/dV$  step of a HoCo dimer (dots: raw data; lines: sigmoid fits). Each data point represents the average from 10 spectra recorded on the same HoCo dimer ( $V_t = 30$  mV,  $I_t = 750$  pA,  $V_{\text{mod,ptp}} = 500$   $\mu$ V,  $T = 0.4$  K). (b) Zeeman plot obtained from measurements on four HoCo dimers adsorbed on 1 ML MgO/Ag(100) (filled triangles) and three HoCo dimers on 2 ML MgO/Ag(100) (filled circles) ( $T = 4$  K). Different colors represent the individual heterodimers. The 0.4 K measurements shown in (a) are included as open black triangles. Error bars represent the standard deviation from  $\geq 5$  measurements on the same heterodimer. The dashed line shows a fit with the spin Hamiltonian described in the text ( $D = -0.47$  meV,  $J = -1.43$  meV,  $g_{Co} = 3.2$ ).

transition is observed suggests that the intensity of the second is below our detection limit. Therefore, we used spin-polarized (SP) STM tips that can enhance the cross section of spin-excitation processes allowing us to probe very weak SES transitions [39,42]. We spin polarized the current by transferring Co atoms to the tip until a signature of spin polarization in the SES of Co is observed (Fig. S3 [18]) [39]. Figure 3(a) shows that the steps at  $\pm 20$  meV are now intense dips, indicative of spin pumping [43], and indeed, an additional pair of symmetric steps at  $\pm 8.1$  meV become apparent [Fig. 3(b)]. Being only 13% of the  $\pm 20$  meV step conductance, this transition would have a conductance variation of merely 1% without SP, and thus, it is obscured by noise in Fig. 1(e). Note that the zero-bias dip in the  $dI/dV$  spectra measured on the surface and the concomitant peak in the corresponding measurement on the

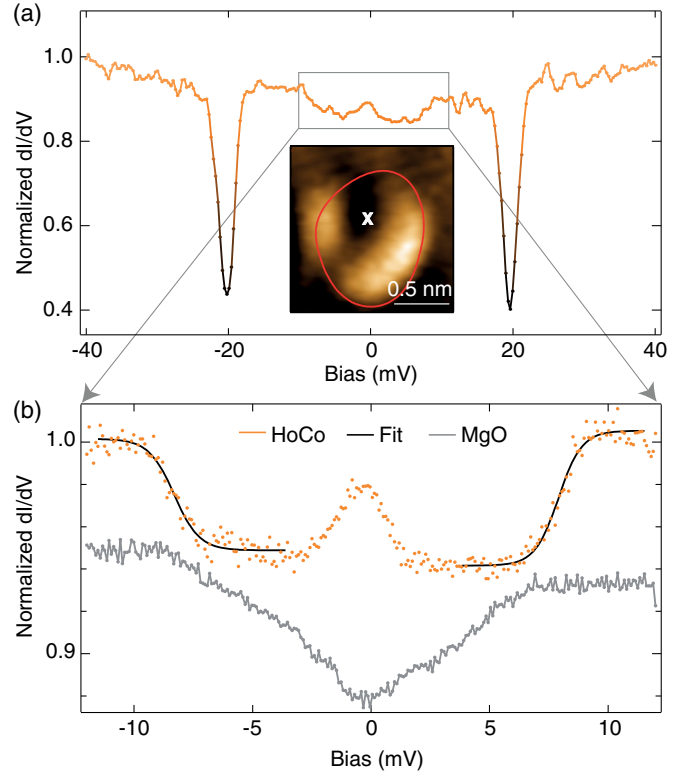


FIG. 3. (a)  $dI/dV$  spectra measured with a spin-polarized tip at the center of a HoCo dimer (dots: measurements, lines: sigmoid fits). Inset shows the corresponding  $dI/dV$  map measured at  $V_t = 20$  mV overlaid with the contour of 15% of the maximum apparent height of the heterodimer. In addition to the jagged inelastic features at  $\pm 20$  meV, a pair of inner steps are detected at about  $\pm 8.1$  meV ( $V_t = 40$  mV,  $I_t = 1$  nA, and  $V_{\text{mod,ptp}} = 500$   $\mu$ V). (b) Zoom on the inner step shown in (a). Each data point represents the average from five acquisitions. ( $V_t = 15$  mV,  $I_t = 300$  pA, and  $V_{\text{mod,ptp}} = 200$   $\mu$ V).  $\mu_0 H = 8$  T and  $T = 0.4$  K for both figures.

dimer may stem from different quantum interference paths of the tunneling electrons in the presence of the SP tip. A similar zero-bias peak has also been observed for Fe atoms on MgO with an SP tip [39].

The observed inelastic features are mapped onto an effective spin Hamiltonian (SH) of the following form:  $\hat{H} = D\hat{S}_z^2 + J(\hat{\mathbf{S}}_{\text{Ho}} \cdot \hat{\mathbf{S}}_{\text{Co}}) + \mu_B [g_{\text{Ho}}\hat{\mathbf{S}}_{\text{Ho}} + g_{\text{Co}}\hat{\mathbf{S}}_{\text{Co}}] \cdot \mu_0 \mathbf{H}$ , where  $D$  is the uniaxial out-of-plane ( $z$ -axis) anisotropy,  $J$  is the Heisenberg exchange coupling between effective Ho and Co spin, and the last term is the Zeeman energy due to the external field acting on both effective spins.

The effective spin values define the level multiplicity of the lowest multiplet. For RE elements the spin-orbit coupling largely dominates over the crystal field and, therefore, the effective spin can be well described using the total magnetic moment (orbital + spin) [44]. Accordingly, for Ho, we consider the  $4f$  occupancy obtained from DFT calculations of 11.02, and deduce the total magnetic moment as the highest possible projection in the  $4f^{11}$

configuration. This yields  $g_{\text{Ho}} = 1.2$  and  $S_{\text{Ho}} = 15/2$ . In contrast, for TMs the hierarchy of interactions is reversed. Consequently, the total moment is no longer a good quantum number [17,39]. In particular, for low symmetry environments, the level multiplicity can be defined by the spin moment only [45,46]. Therefore, for Co, we take the spin magnetic moment  $S_{\text{Co}} = 1$  calculated from DFT, and include the possibility of a nonvanishing orbital component through  $g_{\text{Co}}$ . This leaves  $D$ ,  $J$ , and  $g_{\text{Co}}$  as the only free parameters. Note that the Ho-4*f* and Co-3*d* occupancy in the dimer differ from the respective single atom counterparts [17,33].

Both inelastic steps, as well as the large effective  $g$  factor for the spin excitation at  $\pm 20$  meV, are reproduced with  $D = -0.46 \pm 0.02$  meV (out-of-plane easy axis),  $J = -1.42 \pm 0.05$  meV (ferromagnetic coupling), and  $g_{\text{Co}} = 3.2 \pm 0.1$ . Figure 2(b) illustrates the excellent agreement between the measured (full line) and calculated (dashed line) Zeeman shift of the step energy. A positive  $J$  would yield  $g < 2$ , which contradicts our experimental observation of  $g = 3.1 \pm 0.3$ . The ferromagnetic coupling between the two atoms in the heterodimer is also found in DFT, in contrast to the ferrimagnetic exchange reported for most bulk RE-TM alloys [47]. Note that applying an out-of-plane magnetic field leads to a significantly higher  $g$  factor compared to a free electron value of 2. This suggests an out-of-plane easy axis of the heterodimer, in contrast to the in-plane orientation calculated from DFT.

Figure 4 sketches the ground state and the first two excited states which are accessible in the presence of the  $\Delta S = \pm 1, 0$  selection rules [45]. The two observed transitions are  $|S, S_z\rangle = |17/2, \pm 17/2\rangle \rightarrow |15/2, \pm 15/2\rangle$ , for which we calculate 21.1 meV at 8 T, and  $|17/2, \pm 17/2\rangle \rightarrow |17/2, \pm 15/2\rangle$ , for which our SH yields 8.2 meV at 8 T.

In order to quantify the contribution of each atom to  $S_z$ , we compute the expectation value of  $S_{z,\text{Ho}}$  and  $S_{z,\text{Co}}$  (Supplemental Material [18]) and show them on the right-hand side of Fig. 4. The prominent inelastic transition observed at  $\pm 20$  meV is dominated by an almost 90% reduction of  $S_{z,\text{Co}}$ , whereas the out-of-plane projection of

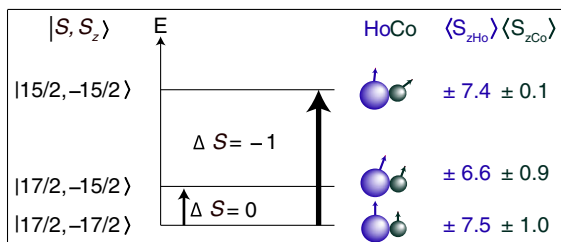


FIG. 4. Schematic of the magnetic sublevels involved in the SES process. The  $\Delta S = -1$  transition (thick arrow) causes the high energy  $dI/dV$  steps and implies a large change in  $S_{z,\text{Co}}$  and, therefore, has a large signal. The low energy steps are due to a  $\Delta S = 0$  transition where  $S_{z,\text{Co}}$  changes only slightly (thin arrow).

the Ho moment is reduced only by a few percent. If we assumed that the tunnel electrons interacted mostly with the TM element, this would explain the larger step height for this transition implying a strong change of  $S_{z,\text{Co}}$ . For the inner steps at  $\pm 8.1$  meV the opposite is true; i.e., the change of the out-of-plane projected overall magnetic moment of the dimer is mostly due to the Ho atom, again in agreement with the observation of these steps having low intensity. Finally, we attribute the large  $g_{\text{Co}} = 3.2$  value to an unquenched orbital moment contribution of  $m_L = 1.2\mu_B$  [18]. This value compares well with previous reports for single surface-supported Co atoms [48,49]. However, it is strongly reduced compared to the maximum orbital moment of Co atoms on MgO [17], due to the lowered symmetry caused by the neighboring Ho atom in the heterodimer.

In conclusion, we detected spin excitations of individual exchange-coupled RE-TM heterodimers. The spectroscopic cross section mostly results from the out-of-plane projected spin variations in the 3*d* element. The possibility of detecting inelastic transitions of magnetic origin in RE based nanostructures allows unprecedented access to their magnetic level diagram, as well as their internal magnetic coupling.

We acknowledge funding from the Swiss National Science Foundation (SNSF) through Grants No. 200020–No. 157081 (A. S.), No. PP00P2\_176866 and No. PZ00P2\_167965 (F. D. N.), No. PZ00P2–No. 142474 (C. W.), and No. IZ73Z0–No. 152406 (S. S.). S. S., Z. S. P., and Ž. Š. acknowledge funding from the Serbian Ministry of Education and Science (Grant No. OI–171033). The DFT calculations were performed at UK (Archer) and Swedish (Beskow) supercomputing facilities, available through Grant No. PRACE DECI–13.

- [1] P. C. M. Gubbens and K. H. J. Buschow, *J. Appl. Phys.* **44**, 3739 (1973).
- [2] I. A. Campbell, *J. Phys. F* **2**, L47 (1972).
- [3] L. T. Baczewski, D. Givord, J. M. Alameda, B. Dieny, J. Nozieres, J. P. Rebouillat, and J. J. Prejean, *Acta Phys. Pol. A* **83**, 629 (1993).
- [4] A. Mishra, W. Wernsdorfer, K. A. Abboud, and G. Christou, *J. Am. Chem. Soc.* **126**, 15648 (2004).
- [5] J. Dreiser, K. S. Pedersen, T. Birk, M. Schau-Magnussen, C. Piamonteze, S. Rusponi, T. Weyhermüller, H. Brune, F. Nolting, and J. Bendix, *J. Phys. Chem. A* **116**, 7842 (2012).
- [6] R. Westerström, J. Dreiser, C. Piamonteze, M. Muntwiler, S. Weyeneth, H. Brune, S. Rusponi, F. Nolting, A. Popov, S. Yang, L. Dunsch, and T. Greber, *J. Am. Chem. Soc.* **134**, 9840 (2012).
- [7] V. Vieru, L. Ungur, and L. F. Chibotaru, *J. Phys. Chem. Lett.* **4**, 3565 (2013).
- [8] R. Westerström, A.-C. Uldry, R. Stania, J. Dreiser, C. Piamonteze, M. Muntwiler, F. Matsui, S. Rusponi,

- H. Brune, S. Yang, A. Popov, B. Büchner, B. Delley, and T. Greber, *Phys. Rev. Lett.* **114**, 087201 (2015).
- [9] A. J. Heinrich, J. A. Gupta, C. P. Lutz, and D. M. Eigler, *Science* **306**, 466 (2004).
- [10] D. Coffey, J. L. Diez-Ferrer, D. Serrate, M. Ciria, C. d. l. Fuente, and J. I. Arnaudus, *Sci. Rep.* **5**, 13709 (2015).
- [11] M. Steinbrecher, A. Sonntag, M. dos Santos Dias, M. Bouhassoune, S. Lounis, J. Wiebe, R. Wiesendanger, and A. A. Khajetoorians, *Nat. Commun.* **7**, 10454 (2016).
- [12] M. Bode, M. Getzlaff, and R. Wiesendanger, *Phys. Rev. Lett.* **81**, 4256 (1998).
- [13] T. Schuh, T. Miyamachi, S. Gerstl, M. Geilhufe, M. Hoffmann, S. Ostanin, W. Hergert, A. Ernst, and W. Wulfhchel, *Nano Lett.* **12**, 4805 (2012).
- [14] T. Miyamachi, T. Schuh, T. Markl, C. Bresch, T. Balashov, A. Stohr, C. Karlewski, S. Andre, M. Marthaler, M. Hoffmann, M. Geilhufe, S. Ostanin, W. Hergert, I. Mertig, G. Schon, A. Ernst, and W. Wulfhchel, *Nature (London)* **503**, 242 (2013).
- [15] T. Balashov, T. Miyamachi, T. Schuh, T. Märkl, C. Bresch, and W. Wulfhchel, *Surf. Sci.* **630**, 331 (2014).
- [16] F. Donati, A. Singha, S. Stepanow, C. Wäckerlin, J. Dreiser, P. Gambardella, S. Rusponi, and H. Brune, *Phys. Rev. Lett.* **113**, 237201 (2014).
- [17] I. G. Rau, S. Baumann, S. Rusponi, F. Donati, S. Stepanow, L. Gragnaniello, J. Dreiser, C. Piamonteze, F. Nolting, S. Gangopadhyay, O. R. Albertini, R. M. Macfarlane, C. P. Lutz, B. A. Jones, P. Gambardella, A. J. Heinrich, and H. Brune, *Science* **344**, 988 (2014).
- [18] See Supplemental Material at <http://link.aps.org/supplemental/10.1103/PhysRevLett.121.257202> for details on MgO preparation, DFT calculations, and the spin-Hamiltonian model, which also includes Refs. [19–32].
- [19] J. Pal, M. Smerieri, E. Celasco, L. Savio, L. Vattuone, and M. Rocca, *Phys. Rev. Lett.* **112**, 126102 (2014).
- [20] B. Bryant, A. Spinelli, J. J. T. Wagenaar, M. Gerrits, and A. F. Otte, *Phys. Rev. Lett.* **111**, 127203 (2013).
- [21] D. Gatteschi, R. Sessoli, and J. Villain, in *Molecular Nanomagnets* (Oxford Scholarship Online, Oxford, 2006).
- [22] W. Wernsdorfer and R. Sessoli, *Science* **284**, 133 (1999).
- [23] K. Blum, *Density Matrix Theory and Applications* (Springer-Verlag, Berlin, Heidelberg, 2012).
- [24] A. Singha, Ph.D. thesis, Ecole Polytechnique Federal de Lausanne, 2017.
- [25] T. Ozaki, *Phys. Rev. B* **67**, 155108 (2003).
- [26] I. Morrison, D. M. Bylander, and L. Kleinman, *Phys. Rev. B* **47**, 6728 (1993).
- [27] OpenMX, open source package for material explorer, <http://www.openmx-square.org/>.
- [28] J. P. Perdew, K. Burke, and M. Ernzerhof, *Phys. Rev. Lett.* **77**, 3865 (1996).
- [29] V. I. Anisimov, J. Zaanen, and O. K. Andersen, *Phys. Rev. B* **44**, 943 (1991).
- [30] H. J. Monkhorst and J. D. Pack, *Phys. Rev. B* **13**, 5188 (1976).
- [31] D. C. Liu and J. Nocedal, *Math. Program.* **45**, 503 (1989).
- [32] N. Ishikawa, M. Sugita, T. Okubo, N. Tanaka, T. Iino, and Y. Kaizu, *Inorg. Chem.* **42**, 2440 (2003).
- [33] F. Donati, S. Rusponi, S. Stepanow, C. Wäckerlin, A. Singha, L. Persichetti, R. Baltic, K. Diller, F. Patthey, E. Fernandes, J. Dreiser, Ž. Šljivančanin, K. Kummer, C. Nistor, P. Gambardella, and H. Brune, *Science* **352**, 318 (2016).
- [34] F. D. Natterer, K. Yang, W. Paul, P. Willke, T. Choi, T. Greber, A. J. Heinrich, and C. P. Lutz, *Nature (London)* **543**, 226 (2017).
- [35] F. D. Natterer, F. Donati, F. Patthey, and H. Brune, *Phys. Rev. Lett.* **121**, 027201 (2018).
- [36] C. Wäckerlin, F. Donati, A. Singha, R. Baltic, S. Rusponi, K. Diller, F. Patthey, M. Pivetta, Y. Lan, S. Klyatskaya, M. Ruben, H. Brune, and J. Dreiser, *Adv. Mater.* **28**, 5195 (2016).
- [37] L. Claude, Ph. D. thesis, École Polytechnique Fédéral de Lausanne, 2005.
- [38] E. Fernandes, F. Donati, F. Patthey, S. Stavrić, Ž. Šljivančanin, and H. Brune, *Phys. Rev. B* **96**, 045419 (2017).
- [39] S. Baumann, F. Donati, S. Stepanow, S. Rusponi, W. Paul, S. Gangopadhyay, I. G. Rau, G. E. Pacchioni, L. Gragnaniello, M. Pivetta, J. Dreiser, C. Piamonteze, C. P. Lutz, R. M. Macfarlane, B. A. Jones, P. Gambardella, A. J. Heinrich, and H. Brune, *Phys. Rev. Lett.* **115**, 237202 (2015).
- [40] W. Paul, K. Yang, S. Baumann, N. Romming, T. Choi, C. P. Lutz, and A. J. Heinrich, *Nat. Phys.* **13**, 403 (2017).
- [41] T. Schuh, T. Balashov, T. Miyamachi, A. F. Takács, S. Suga, and W. Wulfhchel, *J. Appl. Phys.* **107**, 09E156 (2010).
- [42] S. Baumann, Ph. D. thesis, University of Basel, 2015.
- [43] S. Loth, K. von Bergmann, M. Ternes, A. F. Otte, C. P. Lutz, and A. J. Heinrich, *Nat. Phys.* **6**, 340 (2010).
- [44] J. Dreiser, *J. Phys. Condens. Matter* **27**, 183203 (2015).
- [45] C. F. Hirjibehedin, C.-Y. Lin, A. F. Otte, M. Ternes, C. P. Lutz, B. A. Jones, and A. J. Heinrich, *Science* **317**, 1199 (2007).
- [46] A. F. Otte, M. Ternes, K. von Bergmann, S. Loth, H. Brune, C. P. Lutz, C. F. Hirjibehedin, and A. J. Heinrich, *Nat. Phys.* **4**, 847 (2008).
- [47] Y. Janssen, Ph. D. thesis, Universiteit van Amsterdam, 2003.
- [48] P. Gambardella, S. Rusponi, M. Veronese, S. S. Dhesi, C. Grazioli, A. Dallmeyer, I. Cabria, R. Zeller, P. H. Dederichs, K. Kern, C. Carbone, and H. Brune, *Science* **300**, 1130 (2003).
- [49] F. Donati, L. Gragnaniello, A. Cavallin, F. D. Natterer, Q. Dubout, M. Pivetta, F. Patthey, J. Dreiser, C. Piamonteze, S. Rusponi, and H. Brune, *Phys. Rev. Lett.* **113**, 177201 (2014).

## Supplemental Material: Magnetic properties probed in a $4f - 3d$ heterodimer

### SAMPLE PREPARATION

Rare earth elements need special care as they are highly reactive and prone to oxidation. As a first step, a high purity (99.9 %) rod of Ho was cleaned by filing off the oxidized surface layer until a shiny metal surface became visible. In order to minimize its exposure to ambient conditions, the Ho rod was immediately placed into one of the cells of a triple electron-beam evaporator. Similar strategy was followed with a high purity Co rod. After installing the rods in the triple evaporator, it was baked at 150°C for 48 hours. To further ensure purity of our samples, all rods were degassed for several days by operating the evaporator at parameters very close to the ones for actual deposition. The degassing was terminated when no further change in the base pressure was observed after switching the e-beam evaporator on or off.

The Ag(100) single crystal was prepared using several Ar<sup>+</sup> ion sputtering and annealing cycles ( $T = 773$  K,  $p_{\max} = 1 \times 10^{-9}$  mbar). MgO was grown by evaporating Mg from a Knudsen cell onto a clean Ag(100) substrate in a background oxygen pressure of  $1 \times 10^{-6}$  mbar. Prior to this preparation, the Mg source was thoroughly degassed. During MgO growth, the Ag(100) crystal was kept at 773 K. After the Mg evaporation, the Ag(100) surface was allowed to slowly cool down to room temperature at a rate of 22 K/min. The temperature of Ag(100) during deposition and the speed of its post-deposition cool down, determine the thickness and morphology of the MgO layers [25, 26, 36]. The labelling of MgO thickness follows from field emission resonances as shown in ref. [23]. Note that Paul *et al.* use a different thickness labelling [26]. The transfer of samples from the preparation to the STM chamber was *in-situ* in UHV. The atomic species were evaporated onto the sample held in the STM. This implies lowering the STM from the center of the magnet to the sample transfer position and opening the thermal shields [24] which leads to a sample temperature between 13 and 15 K during deposition. At these temperatures both adsorbed atoms are immobile. The amount of Co and Ho deposited (0.015 ML) was chosen to optimize the yield of dimers, while keeping the species still sufficiently far apart to avoid any kind of interaction between them.

### SPECTROSCOPY OF HOMODIMERS

Homodimers of Co and Ho, *i.e.*, Co<sub>2</sub> and Ho<sub>2</sub>, exhibit characteristic inelastic excitations. The  $dI/dV$  steps of Co<sub>2</sub> and their Zeeman shift are shown in Fig. S1. The inset of Fig. S1(a) shows the entire spectrum, while the main figure shows the step for negative polarity and its 0.5 meV shift caused by an increase of the external out-of-plane magnetic field from 1 to 8 T. As expected, the shift is linear in field (Fig. S1(b)). However, it is opposite in sign compared to the one of the  $\pm 20$  meV step of HoCo, namely a field increase lowers the absolute value of the step energy. The reason is either a different orientation of the easy magnetization axis of the total dimer moment, or a different exchange coupling between the two atoms.

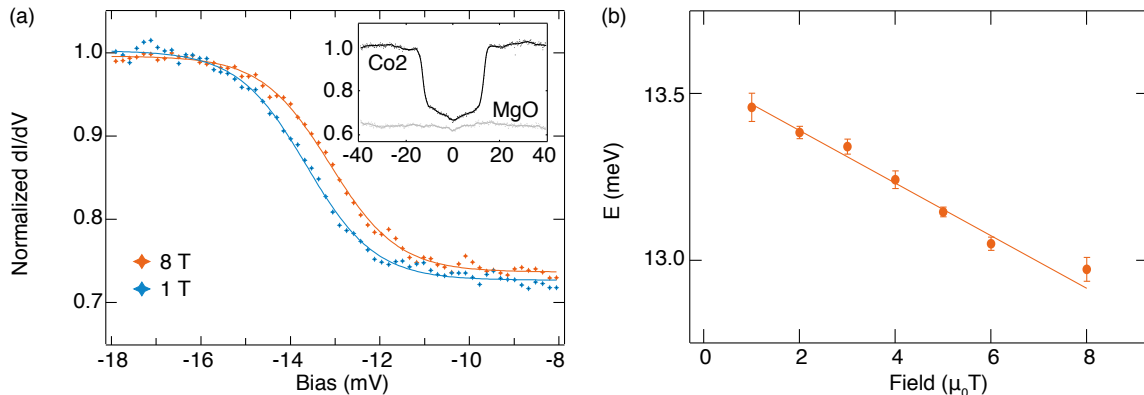


Figure S1. (a) Zoom of the magnetic field dependent  $dI/dV$  spectra of a Co dimer (dots: measurements, lines: sigmoid fits). Inset shows spectrum in the full energy range along with the corresponding background spectra measured on the substrate. The latter is offset by -0.375 units for clarity. ( $V_t = 40$  mV,  $I_t = 250$  pA,  $V_{\text{mod,ptp}} = 1$  mV,  $T = 4.3$  K). (b) Zeeman series of excitation energies, indicating the linear shift of the inelastic feature with the external magnetic field.

Note that the features observed at around  $\pm 5$  meV shift non-monotonically with the magnetic field (inset of Fig. S1(a)). In addition, some low-energy features are also observed in the background spectra, impeding a quantitative analysis of the low-energy features of  $\text{Co}_2$ . Consequently only steps at  $\pm 13$  meV are identified as magnetic excitations and a spin-Hamiltonian simulation would be largely overparametrized in this case.

Figure S2 shows the differential conductance steps observed on  $\text{Ho}_2$ . They are by far the most intense and highest energy steps amongst the three investigated dimer species. In addition, the  $\text{Ho}_2$   $dI/dV$  steps distinguish themselves from the ones recorded on  $\text{Co}_2$  and  $\text{HoCo}$  by the fact that they don't move in an external out-of-plane magnetic field, at least within our detection limits. This indicates either a non-magnetic origin or very strong in-plane magnetic anisotropy in these dimers.

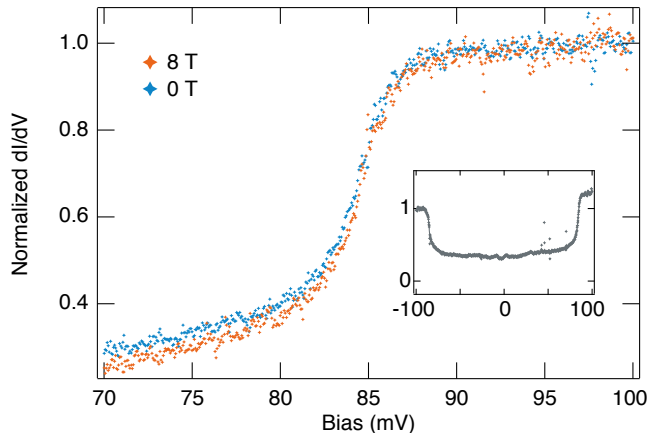


Figure S2. Zoom into the positive bias  $dI/dV$ -step of a Ho dimer. The inset shows the  $dI/dV$  spectrum in the full energy range. The step height is 50 % *i.e.*, the highest amongst the three investigated dimers. Also the excitation energy ( $\pm 85$  meV) is by far the highest ( $V_t = 120$  mV,  $I_t = 1$  nA,  $V_{\text{mod,ptp}} = 200$   $\mu\text{V}$ ,  $T = 0.4$  K).

### SPECTROSCOPY WITH SPIN-POLARIZED TIPS

Typical spectra recorded with a spin-polarized tip are shown in Fig. S3(a) for two Co atoms and one HoCo dimer and in Fig. S3(b) for two acquisitions on the same HoCo dimer. As expected for a spin-polarized tip, these spectra exhibit a strong asymmetry in the differential conductance with respect to bias polarity [29]. Moreover, in all cases the SES steps have very different shape than the ones recorded with non-spin polarized tips as presented in Fig. 1(e). Similar behaviour has been reported for Co atoms on the same surface [28]. The presence of jagged edges instead of simple steps is a signature of spin-pumping which is sensitively probed with spin-polarized tips [28].

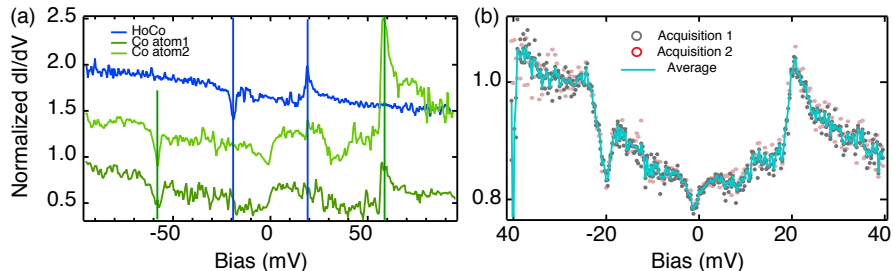


Figure S3. Normalized  $dI/dV$  spectra (a) of two Co atoms and one HoCo dimer with the same tip on 1 ML MgO and (b) for two different acquisitions on another HoCo dimer. Spectra are vertically offset by 0.5 units for clarity in (a). The differential conductance exhibits strong asymmetry with respect to bias polarity in all cases, a typical signature of having a spin-polarized tip. The inelastic steps are strongly deformed, presumably due to spin-pumping. ((a):  $V_{\text{mod,ptp}} = 1$  mV,  $T = 2.0$  K,  $\mu_0 H = 0.2$  T;  $V_t = -150$  mV,  $I_t = 1.5$  nA for Co atoms,  $V_t = 100$  mV,  $I_t = 500$  pA for HoCo dimer, (b)  $V_{\text{mod,ptp}} = 1$  mV,  $T = 0.4$  K,  $\mu_0 H = 1.0$  T,  $V_t = 40$  mV,  $I_t = 1$  nA).

## SIGMOID FITS TO THE CONDUCTANCE STEPS

In order to determine most precisely the position of the inelastic differential conductance steps, we fitted  $dI/dV$  with a sigmoid function using the Fermi-Dirac distribution  $F(x)$  to generate the step:

$$\begin{aligned} f(x) &= A + M(1 - F(x)) \\ &= A + M \left( 1 - \frac{1}{1 + e^{\frac{x-E}{\delta}}} \right). \end{aligned} \quad (\text{S1})$$

$A$  and  $M$  are the baseline and amplitude of the inelastic step, respectively,  $x = eV_t$  is the energy corresponding to the tunnel voltage, and  $E$  the energy of the inelastic step. The broadening of the step  $\delta$  is caused by (a) the lifetime of the excited state involved in the inelastic process, (b) the temperature, and (c) the modulation voltage applied for recording the spectra with Lock-In detection. The fit parameters for the HoCo data shown in Fig. 2(a) and Fig. 3(b) are listed in Table I. Note that the tabulated  $E$  values do not change within our precision if we analyse the numerically derived  $d^2I/dV^2$  data and use a Gaussian profile for fitting it.

Parameters	Fig. 2(a)		Fig. 3(b)	
	1 T	8 T	$V_t < 0$	$V_t > 0$
$E$ (meV)	19.50	20.80	8.30	7.90
$\delta$ (meV)	0.82	0.83	0.53	0.49

Table I. Parameters obtained from the sigmoid fits of HoCo  $dI/dV$  spectra.

Figure 2(b) shows in total 7 different HoCo species, 4 on 1 ML and 3 on 2 ML thick MgO(100) films, each of them represented with different colors. Each symbol results from sigmoid fits of the steps in the respective  $dI/dV$ -data. In Table II we give the individual slopes of  $E(\mu_0 H)$  that correspond to the effective  $g$  factors, as well as the mean value for each MgO(100) thickness.

MgO thickness (ML)	Species	effective $g$ factor	average effective $g$ factor
1	HoCo1	$2.9 \pm 0.3$	$3.1 \pm 0.3$
	HoCo2	$2.9 \pm 0.2$	
	HoCo3	$3.4 \pm 0.3$	
	HoCo4	$3.2 \pm 0.2$	
2	HoCo5	$2.4 \pm 0.4$	$2.5 \pm 0.6$
	HoCo6	$2.5 \pm 0.4$	
	HoCo7	$2.8 \pm 0.9$	

Table II. Effective  $g$  factors measured for the different heterodimers adsorbed on 1 and 2 ML of MgO shown with differently colored symbols in Fig. 2(b). They were obtained by linear regression to the data and are presented in the 3<sup>rd</sup> column with errors representing  $\sigma_i$  of the fit. The last column shows the mean value of  $g$  for each layer thickness together with the corresponding standard deviation calculated as  $\sqrt{\sum_i^n (\sigma_i^2/n)}$ , where  $n$  denotes the total number of cases.

## SPIN HAMILTONIAN MODEL

The effective spin Hamiltonian (SH) model is frequently adopted for describing a system consisting of many spins. In this model, the individual contributions of orbital and spin moments are replaced by an effective spin moment  $S$  that has the same symmetry properties. This approach has been widely used for interpreting inelastic spectroscopy [31, 35, 37] and is also frequently used in molecular magnets [38, 39]. A typical SH takes the following form:

$$\hat{H} = \hat{H}_{CF} + \hat{H}_{Zeeman} . \quad (\text{S2})$$

$\hat{H}_{CF} = D\hat{S}_z^2$  defines the CF along the  $z$  axis, which causes the splitting of the magnetic levels differing in  $S_z$ . Here  $D$  is the uniaxial anisotropy term and the  $z$  component of the spin operator  $\hat{S}$  is defined as  $\hat{S}_z$ . The Zeeman term of



the spin Hamiltonian, describes the interaction of the effective spin with the external magnetic field  $\mu_0\mathbf{H}$ , and this can be written as

$$\hat{H}_{Zeeman} = g\mu_B\hat{\mathbf{S}} \cdot \mu_0\mathbf{H} . \quad (\text{S3})$$

The effective  $g$  factor connects the magnetic field and the effective spin vector;  $\mu_B$  is the Bohr magneton.

Now we turn to the specific case of a heterodimer. In addition to the terms introduced in equation S2, we consider an exchange term,  $\hat{H}_{Exchange}$ , for defining the interaction between the two effective spins of magnitude  $S_{Ho}$  and  $S_{Co}$ . In order to describe the coupled system including all relative orientations of the two individual spins, we employ density matrix formalism [40]. Within this formalism, and according to the Heisenberg coupling scheme,  $\hat{H}_{Exchange}$  can be expressed as:

$$\hat{H}_{Exchange} = J\hat{\mathbf{S}}_{Ho} \cdot \hat{\mathbf{S}}_{Co} , \quad (\text{S4})$$

where  $J$  is the coupling constant and  $\hat{\mathbf{S}}_{Ho}$  and  $\hat{\mathbf{S}}_{Co}$  are the effective spin operators. These operators follow from their usual definitions, however, the respective basis vectors are defined from the product space:

$$\begin{aligned} \hat{\mathbf{S}}_{jHo} &= \hat{S}_j(S_{Ho}) \otimes \mathbb{1}_{2S_{Co}+1} , \\ \hat{\mathbf{S}}_{jCo} &= \mathbb{1}_{2S_{Ho}+1} \otimes \hat{S}_j(S_{Co}) , \\ j &\in \{x, y, z\} . \end{aligned} \quad (\text{S5})$$

Altogether these reduce the effective SH for a system of two coupled spins subject to an out-of-plane magnetic field  $\mu_0\hat{\mathbf{H}}$  as:

$$\hat{H} = D\hat{S}_z^2 + J(\hat{\mathbf{S}}_{Ho} \cdot \hat{\mathbf{S}}_{Co}) + \mu_B[g_{Ho}\hat{S}_{zHo} + g_{Co}\hat{S}_{zCo}] \cdot \mu_0\hat{\mathbf{H}} . \quad (\text{S6})$$

We first diagonalize the SH to obtain the eigen-values and eigen-vectors. The expectation value of an operator is given by tracing the product of the density matrix of the system with the operator itself [40, 41]. Following this, we compute the expectation values of out-of-plane magnetic moments  $\langle\hat{\mathbf{S}}_{zHo}\rangle$ ,  $\langle\hat{\mathbf{S}}_{zCo}\rangle$ , and  $\langle\hat{\mathbf{S}}_z\rangle$ . They are the expected  $z$ -projected moments of Ho and Co atoms, and the  $z$ -projected overall moment of the heterodimer respectively. Finally, the energy distribution of the magnetic levels shown Fig. 4 is produced by plotting the eigen-values of the SH as a function of the respective  $\langle\hat{\mathbf{S}}_z\rangle$  moments.

In order to avoid overparametrization, we consider only first order uniaxial magnetic anisotropy. Note the large  $g$ -factor as well as the position of the inelastic steps can also be reproduced with a non-vanishing first order off-diagonal term. However, SES is only sensitive to  $\Delta S_z = \pm 1, 0$  transitions. Therefore with only two experimentally observed inelastic steps, we can reliably reproduce the lowest part of the full multiplet structure only, without being sensitive to its overall shape. As the in-plane term largely governs the mixing of the states and therefore influences the overall shape of the full multiplet structure, we can not comment with large confidence on the corresponding value.

The SH model is used to reproduce both inelastic steps as well as the experimentally measured  $g$ -factor. Since the excitation at  $\pm 20$  meV is mainly given by the change in Co spin, the  $g$ -factor of Co plays an important role in determining the effective  $g$ -factor of this transition. Therefore the error bar in  $g_{Co}$  is deduced from the error of the linear fit to the Zeeman plot. On the other hand, the coupling parameter  $J$  and anisotropy term  $D$  both determine the splitting of the magnetic levels. Therefore errors in  $J$  and  $D$  indicate the range within which both inelastic steps can be reproduced with a maximum of 3% deviation from their experimentally observed values.

## DFT CALCULATIONS

The non-collinear spin-polarized DFT calculations of the HoCo dimers on 2 ML thin MgO(100) films adsorbed pseudomorphically on Ag(100) were performed with the openMX computer package [42]. We used fully relativistic norm-conserving pseudopotentials [43] to describe the interaction of the ions with valence electrons. The Kohn-Sham wavefunctions were expanded within a basis set of the optimized pseudoatomic orbitals [44]. The exchange-correlation effects were described using the Perdew-Burke-Ernzerhof (PBE) functional [45]. For Ho  $4f$  states we added on-site Coulomb corrections [46] with  $U = 5$  eV, as also used in our previous study of single Ho atoms on the same surface [19]. The MgO(100)/Ag(100) surface was modeled with a  $(3 \times 3)$  unit cell containing nine Mg and nine O atoms per MgO(100) layer. The underlying Ag(100) substrate was represented by a three-layer slab with nine Ag atoms per fcc(100) layer. The supercell calculations were carried out with the theoretically optimized Ag lattice constants of

4.14 Å and a Monkhorst-Pack mesh of 16  $k$ -points was used for sampling of the surface Brillouin zone [47]. Periodically repeated slabs were decoupled by at least 12 Å thick vacuum. Numerical stability of the calculations was increased by populating electronic states according to the Fermi-Dirac distribution at  $T = 300$  K. Atomic positions were relaxed utilizing the Broyden-Fletcher-Goldfarb-Shanno (BFGS) algorithm [48].

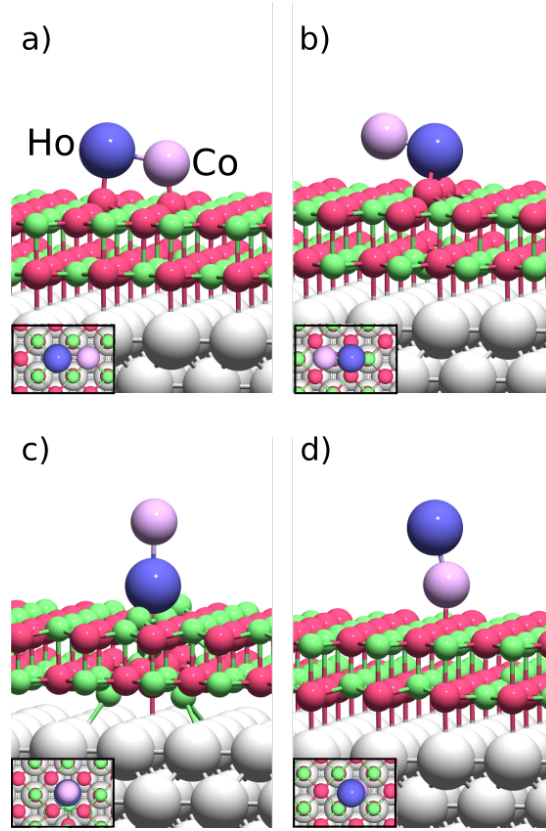


Figure S4. Side views of adsorption geometries of HoCo dimer at 2ML-MgO(100)/Ag(100) considered in our DFT calculations. Insets show top views of the corresponding geometries.

We considered several adsorption geometries of the HoCo dimer on 2 ML MgO(100), as depicted in Fig. S4. Based on the calculated total energies the structure shown in Figs. 1(d) and S4(a) is identified as the most favorable one. The energies of other adsorption geometries with respect to this structure are listed in Table III. Corresponding spin and orbital magnetic moments of Ho and Co as obtained from DFT calculations are also tabulated. Table III shows that in the most stable configuration, the orbital moment of Ho is significantly reduced with respect to the value calculated for the same configuration on 1 ML MgO/Ag(100) (Table V) as well as the values inferred from multiplet calculations for single Ho atoms [19] and experimental values measured for molecular magnets [49]. Similarly for Co, fits to our experimental data using the spin-Hamiltonian model suggest a significantly larger value for the orbital moment compared to what is obtained from our DFT calculations. These suggest a general limitation of DFT for treating correlations in surface supported single atoms, as previously noted for Fe atoms on MgO [25].

For adsorption on 2 ML MgO, our DFT calculations determine a Ho-4*f* occupancy of 11.02. This information is used for deducing the total magnetic moment of 15/2, which is the highest possible projection in the 4*f*<sup>11</sup> configuration. Accounting only for the total moment is justified given the large spin-orbit coupling of Ho, as explained in the main text. All our interpretations about the direction of the easy axis as well as the type of coupling remain unchanged for a different choice of the 4*f* configuration, *e.g.*, 4*f*<sup>10</sup> as reported for single Ho atom on the same surface [41]. In absence of additional experimental inputs, we have chosen to rely on DFT calculated value of 11 in the spin-Hamiltonian model.

In the following, we refer to the almost flat-lying configuration (Fig. S4(a)) for all comparative analysis. In order to understand the effects of charge transfers on the observed magnetic properties of the dimer, we have performed DFT calculations of flat-lying dimers on different substrates. Table IV summarizes the atom-specific and total charge transfers for free dimers (no substrate) and for dimers on 2 ML and 1 ML MgO on Ag(100), as well as on free-

adsorption geometry energy (eV)	Fig. S4(a) 0.00		Fig. S4(b) 0.26		Fig. S4(c) 0.28		Fig. S4(d) 1.27	
	Ho	Co	Ho	Co	Ho	Co	Ho	Co
spin mag. mom. ( $\mu_B$ )	3.00	1.90	4.64	1.61	4.01	2.17	2.84	1.50
orb. mag. mom. ( $\mu_B$ )	1.74	0.22	1.75	0.10	1.86	0.25	3.44	0.21

Table III. Total energies of adsorption geometries of HoCo dimers on 2 ML MgO(100)/Ag(100), relative to the energy of the most favorable structure shown in Fig.S4(a), as well as spin and orbital magnetic moments of Ho and Co atoms.

standing 2 ML MgO (without Ag(100)). For all cases, Ho transfers a fractional charge to the Co atom and, when available, to the substrate. The sum of individual contributions provides the net charge transfer  $\delta q$  from the dimer to the substrate, as shown in the last row of Table IV. The presence of the Ag substrate allows an additional transfer from the HoCo to the substrate of 0.2 – 0.3 electrons with respect to the free-standing MgO case. Note that, the spin magnetism of HoCo dimers in almost flat-configuration is similar on 1 ML and 2 ML MgO/Ag(100), however, the orbital magnetic moments of Ho differ significantly (Table V). Nevertheless, charge transfer does not change the outcome of the spin-Hamiltonian model since the Co spin is hardly influenced by the charge transfer and the Ho is modelled with an effective total moment of  $15/2$ .

	1 ML MgO/Ag(100)	2 ML MgO/Ag(100)	2 ML MgO (no Ag)	no substrate
	$\delta q$ (e)	$\delta q$ (e)	$\delta q$ (e)	$\delta q$ (e)
Co	-0.29	-0.30	-0.39	-0.53
Ho	+1.03	+0.96	+0.82	+0.53
HoCo	+0.74	+0.66	+0.43	0.0

Table IV. Net charge transfers ( $\delta q$ ) from Ho, Co and HoCo to the substrate calculated for flat dimers on 1 ML and 2 ML MgO on Ag(100) and on free-standing 2 ML MgO without Ag substrate underneath. The last column shows the gas phase values for comparison. The values for HoCo are obtained by adding DFT calculated  $\delta q$  values for each atomic species.

	1 ML MgO/Ag(100)		2 ML MgO/Ag(100)		2 ML MgO (no Ag)		no substrate	
	spin	orbital	spin	orbital	spin	orbital	spin	orbital
Co	1.87	0.13	1.90	0.22	1.65	0.14	1.11	0.33
Ho	3.13	6.02	3.00	1.74	2.96	5.69	4.02	2.10

Table V. Spin and orbital magnetic moments of Co and Ho calculated for almost-flat configuration of HoCo dimers on 1 ML and 2 ML MgO on Ag(100). All values are in  $\mu_B$ .

Our DFT calculations suggest that the interatomic distance ( $\delta d$ ) plays an important role in determining the nature of the exchange coupling in the heterodimer. For the most stable dimer structure, the Ho and Co magnetic moments are ferromagnetically coupled, their magnetic moments are nearly collinear, and point along the axis of the dimer. For a fixed interatomic distance of  $\delta d = 2.63$  Å, FM coupling is obtained for both free HoCo and HoCo adsorbed on 2 ML MgO/Ag(100). This suggests that the hybridization with the substrate does not affect the nature of the exchange coupling. The interatomic distance characterizes the orbital overlap and therefore is the leading parameter determining the exchange interaction. The collinear ferromagnetic coupling of the magnetic moments is in agreement with experiment, while the orientation of the overall moment is not. In our experiments a significantly larger  $g$ -factor is observed by applying an out-of-plane magnetic field, indicative of an out-of-plane easy axis of the heterodimer.